Manuscript prepared for Geosci. Model Dev.
with version 2014/07/29 7.12 Copernicus papers of the LaTeX class copernicus.cls.
Date: 12 April 2018

A representation of the collisional ice break-up process in the two-moment microphysics scheme LIMA v1.0 of Meso-NH

Thomas Hoarau[1], Jean-Pierre Pinty[2], and Christelle Barthe[1]

[1]Laboratoire de l'Atmosphère et Cyclones, UMR 8105, CNRS/Météo-France/Université de La Réunion, St Denis, La Réunion, France
[2]Laboratoire d'Aérologie, University of Toulouse/CNRS/UPS, 14 avenue Edouard Belin, F-31400 Toulouse, France

Correspondence to: jean-pierre.pinty@aero.obs-mip.fr

Abstract. The paper describes a switchable parameterization of CIBU (Collisional Ice Break-Up), an ice multiplication process that fits in with the two-moment microphysical scheme LIMA (Liquid Ice Multiple Aerosols). The LIMA scheme with three ice types (pristine cloud ice crystals, snow-aggregates and graupel-hail) was developed in the cloud-resolving mesoscale model Meso-NH.

5   Here the CIBU process assumes that collisional break-up is mostly efficient for small snow-aggregate class of particles with a fragile structure when hit by large and dense graupel particles. The increase of cloud ice number concentration depends on a prescribed number of fragments being produced per collision. This point is discussed and analytical expressions of the newly contributing CIBU terms in LIMA are given.

10   The scheme is run in the cloud resolving mesoscale model Meso-NH to simulate a case of a three-dimension deep convective event with a heavy production of graupel. The consequence of dramatically changing the number of fragments produced per collision is explored in particular to estimate an upper bound of the CIBU effect by examining the rainfall rates. The case of a random number of fragments is also proposed to illustrate the consequence of the uncertainty of this pa-

15   rameter. Finally it is concluded that the assessment of CIBU certainly needs accurate laboratory experiments to check the conditions and to tune the efficiency of the process of ice crystal fragmentation. However the proposed parameterization which is easy to implement in any two-moment microphysics schemes, could be used in this primary form to simulate deep tropical cloud systems where anomalously high concentrations of small ice crystals are preferentially suspected to occur.

1 Introduction

In a series of paper, Yano and Phillips (2011, 2016) and Yano et al. (2016) brought the Collisional Ice Break-Up (hereafter CIBU) process to the fore again as a possible secondary ice production mechanism in clouds. Using an analytical model, they showed that the CIBU could lead to an explosive growth of small ice crystal concentrations. Afterwards Sullivan et al. (2017) tried to include CIBU in a parcel model of six species, assumed to be monodispersed here, in an attempt to make this finding specific. However intriguingly and in contrast to the Hallett-Mossop (hereafter H-M) ice multiplication mechanism[1] (Hallett and Mossop, 1974), the CIBU process was overlooked in cloud physics. So to our knowledge, a contribution of CIBU is never accounted for in the vast majority of the currently used microphysics schemes. Yet, even without absolutely incontestable clues, still missing even in recently published cloud data records[2], the CIBU process is very likely to be active in the case of inhomogeneous cloud regions where ice crystals of different sizes and types are locally mixed (Hobbs and Rangno, 1985; Rangno and Hobbs, 2001). For instance, collisions between large dense graupel growing by riming, and plane vapour-grown dendrites or irregular weakly rimed assemblages are the most conceivable scenario for generating multiple ice debris as envisioned by Hobbs and Farber (1972) and by Griggs and Choularton (1986). So a legitimate quest for a mixed-phase microphysics model such as LIMA (an acronym for Liquid, Ice, Multiple Aerosols, see Vié et al. (2016)) is to find ways to include an ice-ice break-up effect and to characterize its importance, relatively to other ice generating processes like ice heterogeneous nucleation, in the context of a two-moment scheme where number concentrations and mixing ratios of the ice crystals are predicted. At first, our wish to introduce CIBU in a microphysics scheme is essentially motivated by the detection of unexplained high ice water contents that sometimes largely exceed the concentration of ice nucleating particles (Leroy et al., 2015; Field et al., 2017; Ladino et al., 2017).

As recalled by Yano and Phillips (2011), the first few laboratory experiments dedicated to the study of ice collisions were conducted in the 1970s following investigations concerning the promising H-M process. The pioneering work of Vardiman (1978) was a rare experimental reference showing evidence for the mechanical fracturing of natural ice crystals. An interesting issue of the study was to show that the number of fragments was dependent on the shape of the initial colliding crystal and on the momentum change following the collision. According to a concluding remark of Vardiman (1978), this 'secondary' production of ice could lead to concentrations as high as 100 to 1000 times the expected natural concentrations of ice crystals in clouds from heterogeneous nucleation on ice freezing nuclei. Another laboratory study by Takahashi et al. (1995) also revealed a huge production of splinters after collisions between rimed and deposition-grown graupels. However the experimental set-up used there was more appropriate to very big, artificially grown crystals and to large impact velocities because as many as 400 fragments could be obtained.

---

[1]H-M is based on the explosive riming of "big" droplets on graupel particles in a narrow range of temperature

[2]An inventory of the secondary ice production mechanisms is given in Table 1 of Field et al. (2017)

55   For clarity, this study does not focus on cloud conditions leading to an explosive ice multiplication by mechanical break-up in ice-ice collisions (Yano and Phillips, 2011). Neither does it attempt to reformulate this process on the basis of collisional kinetic energy with many empirical parameters as proposed by Phillips et al. (2017), or earlier by Hobbs and Farber (1972) with the breaking energy, mostly applicable to "bin" microphysics schemes. Here, the goal is rather to implement an empir-

60   ical but realistic parameterization of CIBU in the well-suited LIMA scheme (Vié et al., 2016) to cooperate with other microphysical processes (heterogeneous ice nucleation, droplet freezing, H-M process, etc.) to determine the concentration of small ice crystals. Our idealization of CIBU is the formation of cloud ice crystals as the result of asymmetric collisions between big graupel particles and small aggregates followed by the erosion of the latter by the former. The parameterization of

65   CIBU relies on the laboratory observations of Vardiman (1978) to set limits on the number of fragments per collision. However, the large uncertainties attached to this parameter encourage us to run exploratory experiments with several fixed values and also to model the number of fragments by means of a random process with a span of two decades.

     The LIMA scheme is inserted in Meso-NH (Lafore et al., 1998) for several sensitivity experiments

70   to evaluate the importance of the CIBU process and the impact of the tuning i.e., the number of fragments produced per collision. The efficiency of CIBU to dramatically increase the concentration of small ice crystals can be scaled by the ice ice number concentration from nucleation. The case of a three-dimensional continental deep convective storm, the well-known STERAO case analysed by Skamarock et al. (2000), provided a framework for several adjustments of the number of ice

75   fragments. A series of experiments was then performed for the same case to see how much the CIBU process altered the precipitation and the persistence of convective plumes. The question of the number of ice nuclei necessary to initate CIBU (Field et al., 2017; Sullivan et al., 2018) is also tackled. Finally a conclusion is drawn on the usefulness of systematically considering CIBU and other sources of ice multiplication in all mixed-phase two-moment schemes.

80 **2   Introduction of CIBU into the LIMA scheme**

    2.1   General considerations

    In contrast to the work of Yano and Phillips (2011) where large and small graupel particles fuelled the CIBU process, here we consider collisions involving two types of precipitating ice: small aggregates covering pristine ice crystals larger than $\sim$150 μm and large graupel particles. Shocks between

85   graupel particles of different sizes are not considered because according to Griggs and Choularton (1986), the fragmentation of rime is very unlikely to occur in natural clouds. For the sake of simplicity and because the impact velocity of the graupel particles should be well above 1 m s^{-1} to remain in the break-up regime of the aggregates, the particle sizes are selected to enable a substantial occurrence of CIBU.

90   A symbolic form of the equation describing the CIBU process can be written

$$\frac{\partial n_i}{\partial t} = \alpha n_s n_g \tag{1}$$

where n is the number concentration of the cloud ice (subscript "i"), the snow-aggregates ("s") and the graupel particles ("g"). α is the snow-aggregate-graupel collision kernel times $\mathcal{N}_{sg}$, the number of ice fragments produced by collision. The simplest expression of α is

95    $$\alpha = \mathcal{N}_{sg} V_{sg} \frac{\pi}{4} D_g^2 \tag{2}$$

where V_{sg} is the impact velocity of a graupel particle of size D_g at the surface of the aggregate.

In Eq. 2, it is assumed that the size of the aggregate is negligible compared to D_g. V_{sg} is expressed as the difference of fall speed between the colliding graupel and the aggregate target so $V_{sg} = (\rho_{00}/\rho_a)^{0.4} \times (c_g D_g^{d_g} - c_s D_s^{d_s})$ using the generic formula of the particle fall speeds $V_x =$

100   $(\rho_{00}/\rho_a)^{0.4} \times c_x D_x^{d_x}$ with the air density correction of Foote and du Toit (1969) due to the drag force exerted by the particles during their fall. ρ_{00} is the reference air density ρ_a at normal pressure.

As introduced above and suggested in Yano and Phillips (2011), the impact velocity V_{sg} should be such that a minimum value is guaranteed to enable CIBU. An easy way to do this is to restrict the size of the aggregates to the range [D_{smin}=0.2 mm, D_{smax}=1 mm] and to introduce a minimum

105   size of D_{gmin}=2 mm for the graupel particles. The reasons for these choices are discussed in the following. The lower bound value D_{smin} is an estimate that results in the collision efficiency with a graupel particle approaching unity. For $D_s < D_{smin}$, big crystals or aggregates stay outside the path of capture which explains the observation of bimodal ice spectra. Field (2000) reported minimum values of 150-200 μm for D_{trough}, a critical size separating cloud ice and aggregate regimes.

110   The D_{smin} value is also consistent with an upper bound of the cloud ice crystal size distribution that results from the critical diameter of 125 μm to convert cloud ice to snow by deposition (see Harrington et al. (1995) for the original and analytical developments and Vié et al. (2016) for the implementation in LIMA). The choice of D_{smax} and D_{gmin} are dictated by the empirical rule that V_{sg} >1 m s^{-1}. With the setup in LIMA which is $[c_x, d_x] = [5.1, 0.27]$ for "$x = s$" and [124, 0.66]

115   for "$x = g$" in MKS units, one gets V_{sg}>1.26 m s^{-1} at ground level.

The number of fragments $\mathcal{N}_{sg}$ is the critical parameter for ice multiplication. From scaling arguments Yano and Phillips (2011) recommended taking $\mathcal{N}_{sg} = 50$. Recently Yano and Phillips (2016) introduced a notion of random fluctuations into the production of fragments leading to a stochastic equation of the ice crystal concentration due to the realization of a noise process for α (Eq. 2). The

120   parameterization of $\mathcal{N}_{sg}$ as a function of collisional kinetic energy (Phillips et al., 2017) enables a differentiated treatment of the fragmentation of a variety of ice crystals. All these results start from Fig. 6 in Vardiman (1978) which suggests that $\mathcal{N}_{sg}$ is a function of momentum change, ΔM_g, after the collision. As $\Delta M_g \sim 0.1$ g cms^{-1} for D_g=2 mm, the corresponding $\mathcal{N}_{sg}$ lies between 10 (for collision with plane dendrites) and 40 (for rimed spatial crystals). These values are consistent with

125 those found by Yano and Phillips (2011) for rimed assemblages. In conclusion, it is tempting to run
both deterministic and stochastic simulations to test the sensitivity to $\mathcal{N}_{sg}$ but in the range suggested
by laboratory experiments. In the following $\mathcal{N}_{sg}$ was set successively to 0.1 (weak effect) or alterna-
tively one fragment per ten collisions, and 1.0 (moderate effect) and 10.0 (strong effect) fragments
per collision. Additional experiments were performed by first generating a random variable X uni-
130 formly distributed over $[0.0, 1.0]$ and then by applying an empirical formula, $\mathcal{N}_{sg} = 10^{2.0 \times X - 1.0}$,
to generate numbers over two decades $[0.1, 10.0]$ of $\mathcal{N}_{sg}$. The randomization of $\mathcal{N}_{sg}$ reflects the
fact that the number of fragments depends on the positioning of the shock impact, on the tip or on
the body of the fragile particle, and also on the energy lost by the possible rotation of the residual
particle.

2.2 Characteristics of the LIMA microphysics scheme

The microphysics LIMA scheme (Vié et al., 2016) includes a representation of the aerosols as a
mixture of Cloud Condensation Nuclei (CCN) and Ice Freezing Nuclei (IFN) with an accurate budget
equation (transport, activation or nucleation, scavenging by rain) for each aerosol type. The CCN are
selectively activated to produce the cloud droplets which grow by condensation and coalescence to
140 produce the rain drops (Cohard and Pinty, 2000). The ice phase is more complex as we consider
the nucleation by deposition on the IFN and the nucleation by immersion (glaciation of tagged
droplets formed on partially soluble CCN). The homogeneous freezing of the droplets is possible
when the temperature drops below -35° C. The Hallett-Mossop mechanism generates ice crystals
during the riming of the graupel and the snow-aggregates. The H-M efficiency depends sharply on
145 the temperature and on the size distribution of the droplets (Beheng, 1987). The initiation of the
snow-aggregates category is the result of the depositional growth of large pristine crystals beyond a
critical size (Harrington et al., 1995). Aggregation and riming are computed explicitly. Heavily rimed
particles (graupel) can experience a dry or wet growth mode. The freezing of the raindrops by contact
with the small ice crystals is leading to the frozen drops merged with the graupel category. The
150 melting of the snow-aggregates leads to graupel and shedded raindrops while the graupel particles
directly melt into rain. The sedimentation of all particle types is considered. The snow-aggregates
and graupel particles are characterized by their mixing ratios only. The LIMA scheme assumes a
strict saturation of the water vapour over the cloud droplets while the small ice crystals are subject
to super or undersaturated conditions (no instantaneous equilibrium).

2.3 Representation of CIBU in the LIMA scheme

In a 2-moment scheme, the zeroth order (number concentration) and "bth" order (mixing ratio)[3]
moments of the size distributions are computed. So from Eqs.1 and 2 with expansion, the CIBU

---

[3]Ice mixing ratios are computed by integration over the size distribution of the mass of individual particles given by a
mass-size relationship $m(D) = aD^b$, a power law with a non-integer exponent "b"

tendency of the number concentration of the cloud ice N_i (here in $\# \, kg^{-1}$) can be written as:

$$\frac{\partial N_i}{\partial t} = \frac{\mathcal{N}_{sg}}{\rho_{dref}} \frac{\pi}{4} \left(\frac{\rho_{00}}{\rho_{dref}} \right)^{0.4} \int\limits_{D_{smin}}^{D_{smax}} n_s(D_s) \left\{ \int\limits_{D_{gmin}}^{\infty} D_g^2 (c_g D_g^{d_g} - c_s D_s^{d_s}) n_g(D_g) \mathrm{d}D_g \right\} \mathrm{d}D_s \qquad (3)$$

160   where $\rho_{dref}(z)$ is a reference density profile of dry air (Meso-NH is anelastic) and with a further approximation $\rho_a = \rho_{dref}$.

In LIMA, the size distributions follow a generalized gamma law:

$$n(D)\mathrm{d}D = N \frac{\alpha}{\Gamma(\nu)} \lambda^{\alpha\nu} D^{\alpha\nu-1} e^{-(\lambda D)^\alpha} \mathrm{d}D$$

where α and ν are fixed shape parameters, N is the total number concentration and λ is the slope

165   parameter. With the definition of the moments $M_x^{INC}(p; X)$ of the incomplete gamma law given in Appendix A, integration of Eq. 3 leads to:

$$\frac{\partial N_i}{\partial t} = \frac{\mathcal{N}_{sg}}{\rho_{dref}} \frac{\pi}{4} \left(\frac{\rho_{00}}{\rho_{dref}} \right)^{0.4} N_s N_g \times$$

$$\left\{ c_g \left(M_s^{INC}(0; D_{smin}) - M_s^{INC}(0; D_{smax}) \right) \left(M_g(2 + d_g) - M_g^{INC}(2 + d_g; D_{gmin}) \right) \right.$$

170    $$\left. - c_s \left(M_s^{INC}(d_s; D_{smin}) - M_s^{INC}(d_s; D_{smax}) \right) \left(M_g(2) - M_g^{INC}(2; D_{gmin}) \right) \right\} \qquad (4)$$

with $N_s = C_s \lambda_s^{x_s}$ and $N_g = C_g \lambda_g^{x_g}$. The set of flexible parameters used in LIMA is $C_s = 5$, $C_g = 5. \times 10^5$, $x_s = 1$, $x_g = -0.5$. These values were chosen to generalize the classical Marshall-Palmer law, $n(D) = N_0 \exp(-\lambda D)$, a degenerate form of the generalized gamma law when $\alpha = \nu = 1$,

175   leading to a total concentration $N = N_0 \lambda^{-1}$ with a fixed intercept parameter N_0.

Concerning the mixing ratios, the mass of the newly formed cloud ice fragments is simply taken as the product of the mean mass of the pristine ice crystals by the N_i tendency (Eq. 3). The mass loss of the aggregates after collisional break-up is equal to the mass of the ice fragments. The mass of the graupel is unchanged. The mass transfer from aggregates to small ice crystals is constrained by the

180   mass of individual aggregates that may break up completely. This limiting mixing ratio tendency is given by:

$$\frac{\partial r_i}{\partial t} = -\frac{\partial r_s}{\partial t} = \frac{a_s}{\rho_{dref}} \frac{\pi}{4} \left(\frac{\rho_{00}}{\rho_{dref}} \right)^{0.4} \int\limits_{D_{smin}}^{D_{smax}} D_s^{b_s} n_s(D_s) \left\{ \int\limits_{D_{gmin}}^{\infty} D_g^2 (c_g D_g^{d_g} - c_s D_s^{d_s}) n_g(D_g) \mathrm{d}D_g \right\} \mathrm{d}D_s.$$

$$(5)$$

In the above expression the mass of an aggregate of size D_s is given by $a_s D_s^{b_s}$ with a_s=0.02 and b_s=1.9 in LIMA, meaning that aggregates are quasi two-dimensional particles. After integration the

185 mixing ratio tendencies are expressed as:

$$\frac{\partial r_i}{\partial t} = -\frac{\partial r_s}{\partial t} = \frac{a_s}{\rho_{dref}} \frac{\pi}{4} \left(\frac{\rho_{00}}{\rho_{dref}} \right)^{0.4} N_s N_g \times$$

$$\left\{ c_g \left(M_s^{INC}(b_s; D_{smin}) - M_s^{INC}(b_s; D_{smax}) \right) \left(M_g(2 + d_g) - M_g^{INC}(2 + d_g; D_{gmin}) \right) \right.$$

$$\left. - c_s \left(M_s^{INC}(b_s + d_s; D_{smin}) - M_s^{INC}(b_s + d_s; D_{smax}) \right) \left(M_g(2) - M_g^{INC}(2; D_{gmin}) \right) \right\} \quad (6)$$

190

This expression is independent of the number of fragments $\mathcal{N}_{sg}$.

3 Simulation of a 3-dimensional deep convective case

The test case is illustrated by idealized numerical simulations of the 10 July 1996 thunderstorm in the Stratospheric-Tropospheric Experiment: Radiation, Aerosols, and Ozone (STERAO) experiment
195 (Dye et al., 2000). This case is characterized by a multicellular storm which becomes supercellular after 2 hours. The simulations were initialized with the sounding of northeastern Colorado given in Skamarock et al. (2000) and convection was triggered by three 3K-buoyant bubbles aligned along the main diagonal of the X,Y plan in the wind axis. Meso-NH was run for 5 hours over a domain of 320×320 with 1 km-horizontal grid spacing. There were 50 unevenly spaced vertical levels up
200 to 23 km height. With the exception of the wind component, all the fields including microphysics, were transported by an accurate, conservative, positive-definite PPM (Piecewise Parabolic Method) scheme (Colella and Woodward, 1984). There were no surface fluxes but the 3D turbulence scheme of Meso-NH was activated. Open lateral boundary conditions were imposed. The upper level damping layer of the upward moving gravity waves started above 12500 m.
205 The aerosols were initialized as for the simulated squall-line case in Vié et al. (2016). A summary is given in Table 1 for the soluble Cloud Condensation Nuclei (CCN) and for the insoluble Ice Freezing Nuclei (IFN). Homogeneous vertical profiles are assumed for the aerosols. Although the LIMA scheme incorporates size distribution parameters and differentiates the chemical compositions of the CCN and of the IFN, the characteristics of the five aerosol modes are standard for the
210 simulations shown here except for the sensitivity of CIBU to the initial concentration of the IFN which is explored at the end of the study.

3.1 Impact on precipitation

Figure 1 shows the accumulated precipitation at ground level after 4 hours of simulation for the four experiments corresponding to $\mathcal{N}_{sg}$=0.0, 0.1, 1.0 and 10.0. The highest amount of rainfall is
215 obtained when the CIBU process is ignored ($\mathcal{N}_{sg}$=0.0) in Fig. 1a. Then stepping up the CIBU efficiency by decade from $\mathcal{N}_{sg}$=0.1, Fig. 1b-d clearly shows a steady reduction of precipitation and a fine scale modification of the precipitation pattern. Furthermore, Fig. 1d reveals that the spread of

the precipitation field, caused by the motion of the multicellular storm, is significantly reduced when $\mathcal{N}_{sg}$=10.0. The results of Fig. 1 suggest empirically that a plausible range for $\mathcal{N}_{sg}$ is between 0.1 and

220   10.0 fragments per collision. A value lower than 0.1 leads to a negligible effect of CIBU in the simulation, while taking $\mathcal{N}_{sg}>10.0$ has an excessive impact on the storm rainfall (the "$\mathcal{N}_{sg}$=50.0" case is not shown). In complement, Fig 2 shows the results of a simulation, hereafter called "RANDOM", where $\mathcal{N}_{sg}$ is generated by a random process as explained above but providing $0.1 < \mathcal{N}_{sg} < 10.0$. The perturbation caused by CIBU is noticeable in this case too but it remains weak for the precip-

225   itation field. From these first 3D numerical experiments, it can be concluded that CIBU is clearly a disruptive process when $\mathcal{N}_{sg} > 10.0$ fragments per aggregate-graupel collision when taking into account the strong adverse effect on the precipitation field. With $0.1 < \mathcal{N}_{sg} < 10.0$ and furthermore considering $\mathcal{N}_{sg}$ as the realization of a random process, seems to be a more satisfactory approach. Admittedly, the limit $\mathcal{N}_{sg} \sim 10$ is more an order of magnitude but our conclusion is to recommend

230   an upper bound value of $\mathcal{N}_{sg}$ much lower than the former N=50, used by Yano and Phillips (2011) with their notation in the box model.

3.2   Changes in the microphysics

Basically, intensifying the CIBU process by increasing $\mathcal{N}_{sg}$ enhances the concentration of the cloud ice crystals to the detriment of the mass growth of the snow-aggregate category of precipitating ice

235   as these particles are more fragmented when $\mathcal{N}_{sg}$ is increased. However a further effect is possible because the partial mass sink of the snow-aggregate particles also slows down the flux of graupel particles, which form essentially by heavy riming and conversion of the snow-aggregates. This point is now examined by looking at the ice in the high levels of the STERAO cells. Figures 3-5 reproduce the 10 minute average of the mixing ratios r_i, r_s and r_g at 12 km height of the 4 experiments

240   $\mathcal{N}_{sg}$=0.0, 0.1, 1.0 and 10.0 after 4 hours. The increase of the cloud ice mixing ratio with $\mathcal{N}_{sg}$ is clear in the area covered by the $0.2 \, \mathrm{g \, kg^{-1}}$ isocontour in Fig. 3. Simultaneously, a slight decrease of r_s indicating a slow erosion of the mass of the aggregates is visible in Fig. 4. The effect on the graupel (Fig. 5) is even smaller but appears clearly for the case $\mathcal{N}_{sg}$=10.0 where less graupel is found. A last illustration is provided by Fig. 6, showing the number concentration of cloud ice N_i at a higher

245   altitude of 15 km. Again, the increase of N_i follows $\mathcal{N}_{sg}$ with an explosive multiplication of N_i when $\mathcal{N}_{sg}$=10.0 (N_i is well above 1000 crystals $\mathrm{kg^{-1}}$ of dry air in this case). Figure 7 summarizes the behaviour of r_i, r_s, r_g at 12 km height, and of N_i at 15 km height, for the "RANDOM" simulation. The results are those expected but, when comparing these results with Figs 3-6, it is not possible to find microphysics anomalies equivalent to the case where CIBU is not accounted for so "RANDOM"

250   is a full simulation scenario that is intermediate between $\mathcal{N}_{sg}$=1 and $\mathcal{N}_{sg}$=10.

The analysis of the STERAO simulations continues by looking at the vertical profiles of microphysics budgets. The profiles are 10 minute averages of all cloudy columns that contain at least 10^{-3} $\mathrm{g \, kg^{-1}}$ of condensate at any level. The column selection is updated at each time step because of the

evolution and motion of the storm. Figure 8 shows the mixing ratio profiles in three cases: $\mathcal{N}_{sg} =$
0.0, "RANDOM" and $\mathcal{N}_{sg} = 10.0$. A key feature that shows up in Fig. 8a-c is the increase of the r_i
peak value at 11 km altitude. This change is accompanied by a reduction of r_s (more visible between
cases b) and c)) and by a reduction of r_g which clearly stands out at z=8,000 m. The final result is a
decrease of the rain mixing ratio r_r, because rain is mostly fed by the melting of the graupel parti-
cles. The low value of the mean r_r profile, compared to the mixing ratios of the ice phase above, is
explained by the fact that rain is spread over fewer grid points than the ice in the anvil (the mixing
ratio profiles are averaged over the same number of columns).

3.3 Budget of ice mixing ratios

The next step is dedicated to the microphysics tendencies (10 minute average again with the nomen-
clature of the processes provided in Table 3) of the ice mixing ratios in Fig. 9-11 to assess the impact
of the CIBU process. We do not discuss the case of the liquid phase here because the tendencies (not
shown) are not very much affected by CIBU.

As expected, the tendencies of r_i (Fig. 9a-c) are the most affected by the CIBU process. The main
processes, standing out in Fig. 9a when CIBU is not activated, are CEDS (Deposition-Sublimation),
essentially a gain term and AGGS (Aggregation), the main loss of r_i by aggregation with a rate
of 0.5×10^{-3} g kg^{-1} s^{-1}. The loss of r_i by CFRZ (Drop Freezing by Contact) makes a moderate
contribution as some raindrops are present in the glaciated part of the storm. With $\mathcal{N}_{sg}$=RANDOM,
the r_i tendencies are amplified even with a modest contribution of $\sim 0.2 \times 10^{-3}$ g kg^{-1} s^{-1} for
CIBU itself. The growth of AGGS which doubles at 10 km height is caused by the increase in the
SEDI term (Cloud Ice Sedimentation) and the presence of CIBU. The CFRZ contribution is also
increased. The last case, with $\mathcal{N}_{sg}$=10 (Fig. 9c) confirms the general increase of the rates except for
CFRZ, interpreted here as a lack of raindrops.

The budget of the snow/aggregate mixing ratio in Fig. 10 contains many processes of equivalent
importance in the range $\pm 0.05 \times 10^{-3}$ g kg^{-1} s^{-1} but SEDS (Sedimentation of Snow-aggregates)
dominates negatively at $z = 11,000$ m and positively at $z = 7,000$ m. The inclusion of CIBU (Fig.
10b-c) mostly leads to an increase of AGGS, the other processes remaining almost the same. Fi-
nally many processes contribute to the evolution of the graupel mixing ratio profiles (Fig. 11). The
strongest loss is in the GMLT term (Melting of graupel) that converts graupel into rain (down to
-0.3×10^{-3} g kg^{-1} s^{-1}) while the contact freezing of the raindrops (CFRZ) reaches 0.15×10^{-3}
g kg^{-1} s^{-1}. The sedimentation term SEDG (Sedimentation of Graupel) lies between -0.3×10^{-3}
g kg^{-1} s^{-1} at $z = 10,000$ m and 0.15×10^{-3} g kg^{-1} s^{-1} at 5,000 m. Another noticeable effect is
the sign change of DEPG (Growth of Graupel by Deposition, $\pm 0.07 \times 10^{-3}$ g kg^{-1} s^{-1}) showing
that the water vapour is super(under)saturated above(below) z=7,000 m on average. The relative
importance of these processes does not change very much when CIBU is increased but tendencies

weaken. In summary, the impact of CIBU is modest for the microphysics mixing ratios. The increase
of ice fragments in r_i is approximately compensated by an increase of AGGS (see Fig. 9 and 10).

3.4 Budget of cloud ice concentration

The next point examined is the behaviour of the cloud ice number concentration according to the
strength of the CIBU process after 4 hours of simulation. Figure 12 shows that the altitude of the
N_i peak value decreases when $\mathcal{N}_{sg}$ increases. In the absence of CIBU ($\mathcal{N}_{sg} = 0$), the origin of N_i is
the heterogeneous nucleation processes on insoluble IFN and coated IFN (nucleation by immersion)
which are more efficient at low temperature. They provide a mean peak value $N_i = 400$ kg^{-1} at
$z = 11{,}500$ m. In contrast, the $\mathcal{N}_{sg} = 10$ case (here scaled by $\times 0.1$ for plotting reasons) keeps the
trace of an explosive production of cloud ice concentration, $N_i = 7{,}250$ kg^{-1}, due to CIBU. The
altitude of the maximum of N_i in this case ($z = 10{,}000$ m) is consistent with the location of the
maximum value of the $r_s \times r_g$ product (see Fig. 8). The "RANDOM" simulation produces $N_i =$
1100 kg^{-1} at $z = 11{,}000$ m, a number concentration that is an order of magnitude lower. Table 2
reports the peak amplitude of the N_i profiles as a function of $\mathcal{N}_{sg}$ but after 3 hours of simulation
when the CIBU rate is strongly dominant. Additional cases were run to cover $0.1 < \mathcal{N}_{sg} < 50$ with a
logarithmic progression above $\mathcal{N}_{sg} = 1.0$. The CIBU enhancement factor, $\mathrm{CIBU}_{\mathrm{ef}}$, is computed as
$N_i(\mathcal{N}_{sg})/N_i(\mathcal{N}_{sg} = 0) - 1$ as $N_i(\mathcal{N}_{sg} = 0)$ stands as a baseline not affected by CIBU. The results
clearly show that the growth of N_i is fast when $\mathcal{N}_{sg}$ reaches ~ 5.0 ($\mathrm{CIBU}_{\mathrm{ef}}$ switches from 135% to
913% when $\mathcal{N}_{sg}$ moves from 2.0 to 5.0). Taking $\mathcal{N}_{sg} = 50$ leads to a tremendously high N_i peak
value.

The N_i tendencies are the subject of Fig. 13. Many processes are involved during the temporal
integration of N_i. The $\mathcal{N}_{sg} = 0$ case confirms the importance of the heterogeneous nucleation pro-
cess by deposition, HIND, (refer to Table 3) and to a lesser degree by immersion (HINC) at 8 km
height. HIND peaks at three altitudes with two sources of IFN (Table 1). This case also reveals the
importance of the HMG (Hallett-Mossop on Graupel, 1.3 kg^{-1}s^{-1}) and HMS (Hallett-Mossop on
Snow, 0.85 kg^{-1}s^{-1}) processes. Here, we consider that H-M also operates for the snow-aggregates
because this category of ice is prone to light riming, like the graupel particles, in the case of water su-
percooling. These processes are first compensated by AGGS (capture of cloud ice by the aggregates).
There is also a loss of cloud ice due to CFRZ and CEDS with the full sublimation of individual cloud
ice crystals that replenish the IFN reservoir. The sedimentation profile transports ice from cloud top
(SEDI<0) to mid-level cloud (SEDI>0). Then taking $\mathcal{N}_{sg}$ = RANDOM shows the domination of the
CIBU process, which reaches 2.5 kg^{-1}s^{-1} at 5 km height. The enhancement of HIND at cloud top
can also be noted. The CIBU source of ice crystals is balanced by an increase of AGGS and, above
all, of CEDS (here CEDS represents the sublimation of the ice crystal concentration when detrained
in the low level of the cloud vicinity, below the anvil for instance). Finally, the $\mathcal{N}_{sg} = 10$ case demon-

strates the reality of the exponential-like growth of N_i because the three main driving terms CIBU, CEDS and AGGS are growing at a similar rate that is multiplied by a factor 5, approximately.

3.5 Sensitivity to the initial concentration of freezing nuclei

The purpose of the last series of experiments was to look more closely at the sensitivity of the cloud ice concentration to N_{IFN}, the initial concentration of the IFN. Numerical simulations were run with N_{IFN} decreasing by decades from 100 dm^{-3} to 0.001 dm^{-3} for each IFN mode (see Table 1). Two different cases were considered. In the first one, CIBU was activated with the RANDOM set-up while, in the second, CIBU effects were ignored. All the results are summarized in the plots of Fig. 14.

Figure 14a shows that N_i concentrations did not change very much for a wide range of N_{IFN} concentrations, which were scanned by decades. This clearly illustrates the predominance of the CIBU effect for current IFN concentrations, which disconnects N_i concentrations from the underlying abundance of IFN particles. In this vein, the small hump superimposed on all profiles at 5,000 m height reveals a residual effect of the Hallett-Mossop process. A remarkable feature is also that a fairly low IFN concentration (N_{IFN} = 0.001 dm^{-3}) suffices to initiate the CIBU process and to reach $N_i \sim 500$ kg^{-1}. In contrast and in the absence of CIBU (Fig. 14b), the N_i profiles show a sensitivity to IFN nucleation that is, indeed, difficult to interpret because of the non-monotonic trend of the N_i profiles with respect to N_{IFN}. Some insight can be gained by checking the concentration of the nucleated IFN of the first IFN mode (dust particles). In Fig. 14c, the IFN profiles are rescaled (multiplication by an appropriate numbers of powers of ten) to be comparable. Here this is equivalent to computing an IFN nucleation efficiency. The important result here is that the number of nucleated IFN evolves in close proportion to the initially available IFN concentrations, meaning that the nucleating properties of the IFN do not depend on the IFN concentration as expected. The last plot (Fig. 14d) reproduces the normalized differences of N_i profiles between twin simulations performed with CIBU and without CIBU. Even if simulations made with the same initial concentration N_{IFN}, diverge because of additional non-linear effects (vertical transport, enhanced or reduced cloud ice sink processes), the figure gives a flavour of the bulk sensitivity of CIBU to the IFN. The enhancement ratio due to CIBU remains low (less than 1 for $N_{IFN} \sim 100$ dm^{-3}) but can reach a factor of 20 at 9,000 m height in the case of moderate IFN concentration i.e. $N_{IFN} \sim 1$ dm^{-3}. The behaviour of LIMA can be explained in the sense that increasing N_{IFN} too much leads to smaller pristine crystals that need a longer time to grow because the conversion to the next category of snow-aggregates is size-dependent (see Harrington et al. (1995) and Vié et al. (2016)). On the other hand, a low concentration of N_{IFN} initiates fewer snow-aggregate and thus less graupel particles, so the whole CIBU efficiency is also reduced. Consequently, this study confirms the essential role of CIBU to compensate for IFN deficit when cloud ice concentrations are building up.

4 Summary and perspectives

360   The aim of this work was to study a comprehensive parameterization of the Collisional Ice Break-Up for a bulk 2-moment microphysics scheme running in a cloud resolving mesoscale model (Meso-NH in our case). While the process is strongly suspected to occur in real clouds, it is not included in current bulk microphysics schemes. Because of uncertainties, the present parameterization has been kept as simple as possible. It considers only collisions between small aggregates and large

365   dense graupel particles. The number of ice fragments that results from a single shock, $\mathcal{N}_{sg}$, is a key parameter which is only estimated from very few past experiments (Vardiman, 1978). A merit of this study is to provide an upper bound to the value of $\mathcal{N}_{sg}$ because of the sensitivity of $\mathcal{N}_{sg}$ to the simulated precipitation. We found that taking $\mathcal{N}_{sg} > 10$ reduces significantly the precipitation at the ground. This is not acceptable since most of the cloud schemes (running without CIBU process)

370   are tuned for quantitative precipitation forecasts. Furthermore, we suggest to consider $\mathcal{N}_{sg}$ as the realization of a random process because delicate radiating crystals undergoing fragmentation lead to a variety of crystals with a missing arm or to many irregular fragments as illustrated and discussed by Hobbs and Farber (1972). As a result it has been shown, for instance, that running with $\mathcal{N}_{sg} > 10$ in the STERAO deep convection test case, dramatically alters the precipitation at the ground because

375   the conversion of cloud ice crystals into precipitating ice is slowed down. Simultaneously, a major expected effect of CIBU is clearly to increase the number concentration of small ice crystals.

    The microphysics perturbation due to the activation of CIBU has been studied by looking at the profiles of the mixing ratios, ice concentrations and corresponding budget terms. In particular, the CIBU effect on the pristine ice and aggregate mixing ratios is compensated by an enhancement of

380   the capture of the small crystals by the aggregates. The sensitivity of the ice concentration to $\mathcal{N}_{sg}$ is demonstrated with a mean multplication factor as high as 25 for $\mathcal{N}_{sg} = 10$. The last study on the sensitivity of the simulations to the initial IFN concentration showed that CIBU was mostly efficient for current IFN concentrations of ~ 1 dm^{-3}. Furthermore the CIBU process was still active for very low IFN concentrations, down to 0.001 dm^{-3}, which were sufficient to initiate the ice phase.

385   The proposed parameterization is very easy to implement and to evaluate in other microphysics schemes where the growth of precipitating ice is represented differently. The tuning of the scheme can be revised as soon as laboratory experiments are available for fixing more precisely the sizes and the shapes of the crystals that break following collisions and to estimate the variety of fragment numbers more accurately. However, as microphysics schemes are now used to produce quantitative

390   precipitation forecasts, it is also imperative to check that the production of rain is not too much altered by an overstimated CIBU effect.

    With new imagers, counters and improvements in data analysis (Ladino et al., 2017), more and more evidence is being presented that ice multiplication production is a dominant process in natural clouds. However, the explanation of anomalously high ice crystal concentrations is difficult to link

395   to a precise process (Rangno and Hobbs, 2001; Field et al., 2017). So the next step in the LIMA

scheme is to introduce the shattering of the raindrops during freezing as proposed by Lawson et al. (2015) and to compare with CIBU, because the basic ingredients, raindrops and small ice crystals, leading to a different ice multiplication process are not the same. Then, the final task is to check that microphysics schemes with all known sources of small ice crystals, nucleation and secondary

400 ice production, are able to cooperate and to reproduce observed ice concentrations which can reach very high values (units of cm^{-3}) in deep convective clouds but without convincing explanation yet. Quantitative cloud data gathered in the tropics during HAIC/HIWC (High Altitude Ice Crystals/ High Ice water Content) field project (Leroy et al., 2015; Ladino et al., 2017) could be a starting point to evaluate high resolution cloud simulations with high ice contents.

405 **5 Code availability**

The Meso-NH code is publicly available at http://mesonh.aero.obs-mip.fr/mesonh51. Here the model development and the simulations were made with version "MASDEV5-1 BUG2". The modifications brought to the LIMA scheme (v1.0) are available upon request from Jean-Pierre Pinty and next in the Supplement related to this article and available at http://doi.org/10.5281/zenodo.1078527.

410 **Appendix A: Moments of the gamma and incomplete gamma functions**

The pth moment of the generalized gamma function (see definition in the text) is

$$M(p) = \int_0^\infty D^p n(D) \mathrm{d}D = \frac{\Gamma(\nu + p/\alpha)}{\Gamma(\nu)} \frac{1}{\lambda^p} \tag{A1}$$

where the gamma function is defined as:

$$\Gamma(x) = \int_0^\infty t^{x-1} e^{-t} \mathrm{d}t. \tag{A2}$$

415   The pth moment of the incomplete gamma function is written

$$M^{INC}(p; X) = \int_0^X D^p n(D) \mathrm{d}D. \tag{A3}$$

The algorithm of the "GAMMA_INC$(p; X)$" function (Press et al., 1992) is useful to tabulate $M^{IN}(p; X) \times \Gamma(p)$ in addition to the "GAMMA" function algorithm of Press et al. (1992). A change of variable is necessary to take the generalized form of the gamma size distributions into account.

420 As a result, $M^{INC}(p; X)$ is written:

$$M^{INC}(p; X) = M(p) \times \text{GAMMA\_INC}(\nu + p/\alpha; (\lambda X)^\alpha) \tag{A4}$$

with $M(p)$ given by Eq. A1.

Acknowledgements. J.-P. Pinty wishes to thank V. Phillips for discussions about his original work on the topic. This work was done during the PhD of T. Hoarau who is financially supported by Reunion Island Regional Council and the European Union Council. T. Hoarau thanks University of La Réunion for supporting a short stay at Laboratoire d'Aérologie. Mrs Susan Becker corrected the English of the manuscript. Preliminary computations were performed on the 36 node home-made cluster of Lab. Aérologie. J.-P. Pinty acknowledges CALMIP (CALcul MIdi-Pyrénés) of the University of Toulouse for access to the "Eos" supercomputer where useful additional simulations were performed. T. Hoarau and C. Barthe acknowledge the GENCI ressources for access to the "Occigen" supercomputer. The authors thank the reviewers for their pertinent comments which helped to improved a lot the first version of the manuscript.

References

Colella, P. and Woodward, P.: The piecewise parabolic method (PPM) for gas-dynamical simulations, J. Comput. Phys., 54, 174–201, 1984.

Dye, J. E., Ridley, B. A., Skamarock, W., Barth, M., Venticinque, M., Defer, E., Blanchet, P., Théry, C., Laroche, P., Baumann, K., Hubler, G., Parrish, D. D., Ryerson, T., Trainer, M., Frost, G., Holloway, J. S., Matejka, T., Bartels, D., Fehsenfeld, F. C., Tuck, A., Rutledge, S. A., Lang, T., Stith, J., and Zerr, R.: An overview of the Stratospheric-Tropospheric Experiment: Radiation, Aerosols, and Ozone (STERAO)-Deep Convection experiment with results for the July 10, 1996 storm, J. Geophys. Res., 105, 10,023–10,045, doi:10.1029/1999JD901116, 2000.

Field, P. R.: Bimodal ice spectra in frontal clouds, Quart. J. Roy. Meteor. Soc., 126, 379–392, doi:10.1002/qj.49712656302, 2000.

Field, P. R., Lawson, R. P., Brown, P. R. A., Lloyd, G., Westbrook, C., Moisseev, D., Miltenberger, A., Nenes, A., Blyth, A., Choularton, T., Connolly, P., Buehl, J., Crosier, J., Cui, Z., Dearden, C., DeMott, P., Flossmann, A., Heymsfield, A., Huang, Y., Kalesse, H., Kanji, Z. A., Korolev, A., Kirchgaessner, A., Lasher-Trapp, S., Leisner, T., McFarquhar, G., Phillips, V., Stith, J., and Sullivan, S.: Secondary ice production: current state of the science and recommendations for the future, Meteor. Monogr., 58, 7.1–7.20, doi:10.1029/AMSMONOGRAPHS-D-16-0014.1, 2017.

Foote, G. B. and du Toit, P. S.: Terminal velocity of raindrops, J. Appl. Meteor., 8, 249–253, 1969.

Griggs, D. G. and Choularton, T. W.: A laboratory study of secondary ice article production by the fragmentation of rime and vapour-grown ice crystals, Quart. J. Roy. Meteor. Soc., 112, 149–163, doi:10.1002/qj.49711247109, 1986.

Hallett, J. and Mossop, S. C.: Production of secondary ice particles during the riming process, Nature, 249, 26–28, doi:10.1038/249026a0, 1974.

Harrington, J. Y., Meyers, M. P., Walko, R. L., and Cotton, W. R.: Parameterization of Ice Crystal Conversion Processes Due to Vapor Deposition for Mesoscale Models Using Double-Moment Basis Functions. Part I: Basic Formulation and Parcel Model Results, J. Atmos. Sci., 52, 4344–4366, doi:10.1175/1520-0469(1995)052<4344:POICCP>2.0.CO;2, 1995.

Hobbs, P. V. and Farber, R. J.: Fragmentation of ice particles in clouds, J. Rech. Atmos., 6, 245–258, 1972.

Hobbs, P. V. and Rangno, A. L.: Ice particle concentrations in clouds, J. Atmos. Sci., 42, 2523–2549, 1985.

Ladino, L. A., Korolev, A., Heckman, I., Wolde, M., Fridlind, A. M., and Ackerman, A. S.: On the role of ice-nucleating aerosol in the formation of ice particles in tropical mesoscale convective systems, Geophys. Res. Lett., 44, doi:10.1002/2016GL072 455, 2017.

Lafore, J. P., Stein, J., Asencio, N., Bougeault, P., Ducrocq, V., Duron, J., Fischer, C., Héreil, P., Mascart, P., Masson, V., Pinty, J.-P., Redelsperger, J.-L., Richard, E., and Vila-Guerau de Arellano, J.: The Meso-NH atmospheric simulation system. Part I: adiabatic formulation and control simulations, Annales Geophysicae, 16, 90–109, doi:10.1007/s00585-997-0090-6, 1998.

Lawson, R. P., Woods, S., and Morrison, H.: The microphysics of ice and precipitation development in tropical cumulus clouds, J. Atmos. Sci., 72, 2429–2445, doi:10.1175/JAS-D-14-0274.1, 2015.

Leroy, D., Fontaine, E., Schwarzenboeck, A., Strapp, J. W., Lilie, L., Delanoe, J., Protat, A., Dezitter, F., and Grandin, A.: HAIC/HIWC Field Campaign - Specific findings on PSD microphysics in high IWC regions

from in situ measurements: median mass diameters, particle size distribution characteristics and ice crystal shapes, SAE Technical Paper, doi:10.4271/2015-01-2087, 2015.

Phillips, V. T., Yano, J.-I., and Khain, A.: Ice multiplication by break-up in ice-ice collisions. Part I: Theoretical
475   formulation, J. Atmos. Sci., 74, 1705–1719, doi:10.1175/JAS-D-16-0224.1, 2017.

Press, W. H., Teukolsky, S. A., Vetterling, W. T., and Flannery, B. P.: Numerical Recipes in FORTRAN: The Art of Scientific Computing, Cambridge University Press, New-York, 1992.

Rangno, A. L. and Hobbs, P. V.: Ice particles in stratiform clouds in the Arctic and possible mechanisms for the production of high ice concentrations, J. Geophys. Res., 106, 15 065–15 075, 2001.

480   Skamarock, W. C., Powers, J. G., Barth, M., Dye, J. E., Matejka, T., Bartels, D., Baumann, K., Stith, J., Parrish, D. D., and Hubler, G.: Numerical simulations of the July 10 Stratospheric-Tropospheric Experiment: Radiation, Aerosol, and Ozone/Deep Convection Experiment convective system: Kinematics and transport, J. Geophys. Res., 105, 19,973–19,990, 2000.

Sullivan, S. C., Hoose, C., and Nenes, A.: Investigating the contribution of secondary ice production to in-cloud
485   ice crystal numbers, J. Geophys. Res., 122, doi:10.1002/2017JD026 546, 2017.

Sullivan, S. C., Hoose, C., Kiselev, A., Leisner, T., and ²Nenes, A.: Initiation of secondary ice production in clouds, Atmos. Chem. Phys., 18, doi:10.5194/acp–18–1593–2018, 2018.

Takahashi, T., Nagao, Y., and Kushiyama, Y.: Possible high ice particle productionduring graupel-graupel collisions, J. Atmos. Sci., 52, 4523–4527, 1995.

490   Vardiman, L.: The generation of secondary ice particles in clouds by crystal–crystal collision, Journal of the Atmospheric Sciences, 35, 2168–2180, doi:1520-0469(1978)035<2168:TGOSIP>2.0.CO;2, 1978.

Vié, B., Pinty, J.-P., Berthet, S., and Leriche, M.: LIMA (v1.0): A quasi two-moment microphysical scheme driven by a multimodal population of cloud condensation and ice freezing nuclei, Geoscientific Model Development, 9, 567–586, doi:10.5194/gmd-9-567-2016, 2016.

495   Yano, J.-I. and Phillips, V. T.: Ice–Ice Collisions: An Ice Multiplication Process in Atmospheric Clouds, J. Atmos. Sci., 68, 322–333, doi:10.1175/2010JAS3607.1, 2011.

Yano, J.-I. and Phillips, V. T.: Explosive Ice Multiplication Induced by multiplicative-Noise fluctuation of Mechanical Break-up in Ice-Ice Collisions, J. Atmos. Sci., 73, 4685–4697, doi:10.1175/JAS-D-16-0051.1, 2016.

Yano, J.-I., Phillips, V. T., and Kanawade, V.: Explosive ice multiplication by mechanical break-up in ice–ice
500   collisions: a dynamical system-based study, Quart. J. Roy. Meteor. Soc., 142, 867–879, doi:10.1002/qj.2687, 2016.

CCN	Aitken mode	Accumulation mode	Coarse mode
N (cm^{-3})	300	140	50
d_X (µm)	0.23	0.8	2.0
σ_X	2.0	1.5	1.6

IFN	Dust mode	BC+Organics mode
N (dm^{-3})	10	10
d_X (µm)	0.8	0.2
σ_X	2.0	1.6

Table 1. Background CCN and IFN configuration for the STERAO idealized case simulations.

$\mathcal{N}_{sg}$ (no unit)	0.0	0.1	1.0	2.0	5.0	10.0	20.0	50
N_i (#kg^{-1})	790	940	1,160	1,860	8,000	25,670	62,010	112,740
CIBU$_{\text{ef}}$ (%)	0	19	47	135	913	3149	7749	14171

Table 2. After 3 hours of simulation, maximum value of the cloud ice number concentration $N_{i_{max}}$ as a function of the number of fragments produced per snow/aggregate-graupel collision $\mathcal{N}_{sg}$. The last row is the CIBU enhancement factor CIBU$_{\text{ef}}$ in percent (see text).

Process Acronym	Description
ACC	Raindrop accretion on snow to produce graupel
AGGS	Snow growth by capture of cloud ice
BERFI	Growth of cloud ice by Bergeron-Findeisen process
CEDS	Deposition/sublimation of water vapour on cloud ice
CFRZ	Raindrop Freezing by contact with cloud ice
CIBU	Snow break-up by collision with graupel
CMEL	Conversion Melting of snow into graupel
CNVI	Decreasing snow converted back to cloud ice
CNVS	Growing cloud ice converted into snow
DEPG	Water vapour deposition on graupel
DEPS	Water vapour deposition on snow
DRYG	Graupel dry growth (water can freeze fully)
HINC	Heterogeneous nucleation by immersion
HIND	Heterogeneous nucleation by deposition
HONC	Homogeneous freezing of the cloud droplets
HONH	Haze homogeneous freezing
HMG	Droplet riming and Hallett-Mossop process on graupel
HMS	Droplet riming and Hallett-Mossop process on snow
HMS	Water vapour deposition on snow
IMLT	Melting of cloud ice
RIM	Riming of cloud droplets on snow to produce graupel
SEDI	Sedimentation of cloud ice, snow or graupel
WETG	Graupel wet growth (water is partially frozen)

Table 3. Nomenclature of the microphysics processes of the budget profiles.
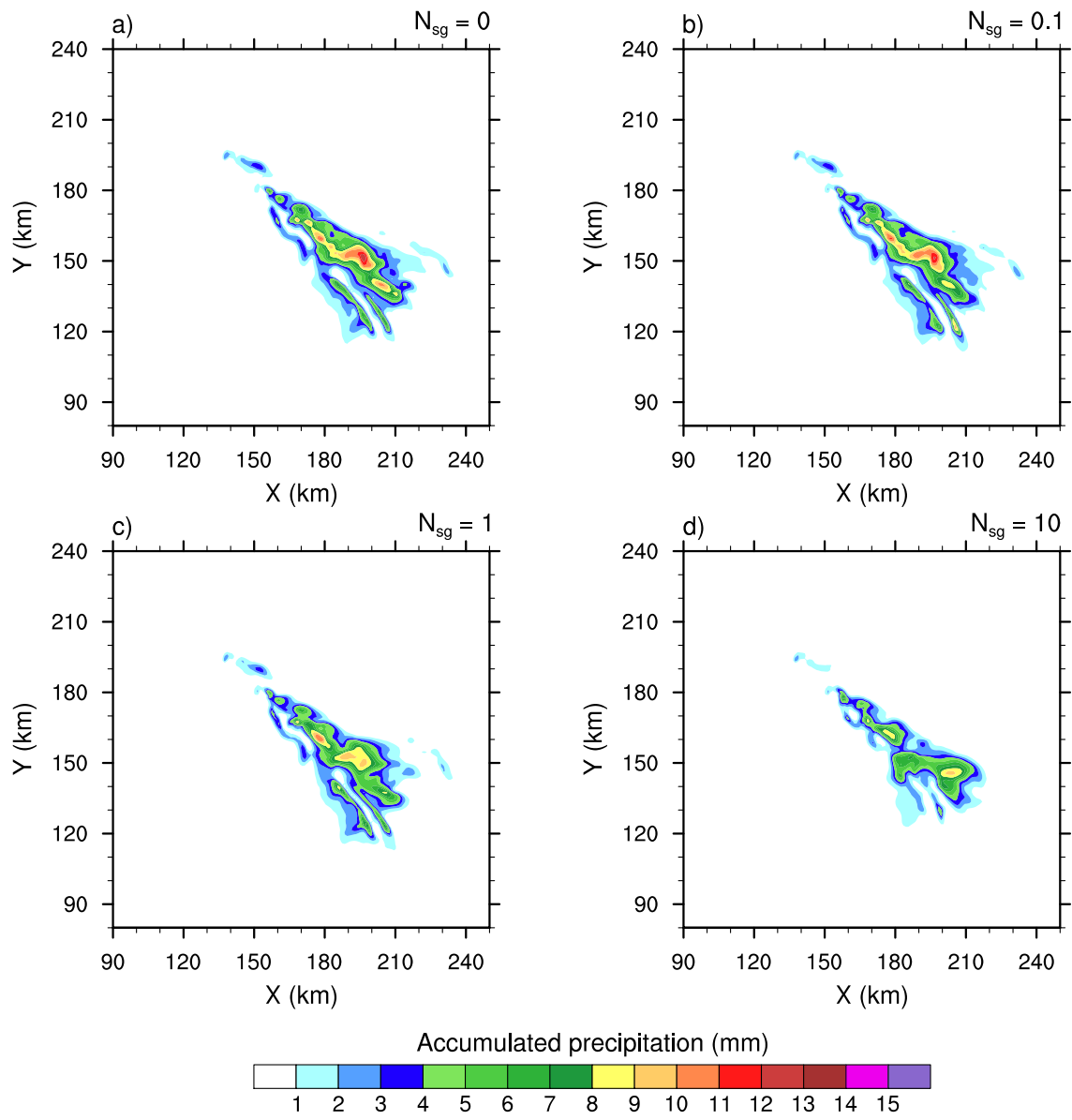
Figure 1. 4-h accumulated precipitation of the STERAO simulations where a) to d) refers to cases with $\mathcal{N}_{sg}$=0.0, 0.1, 1.0 and 10.0 ice fragments per collision, respectively. The plots are for a fraction of the computational domain.
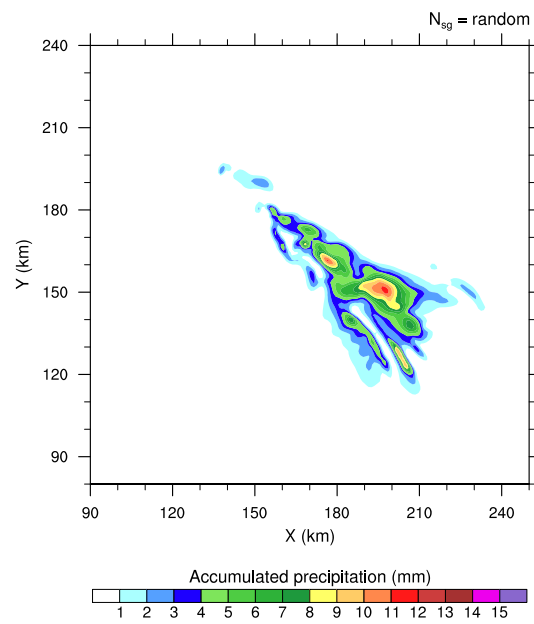
Figure 2. Same as Fig. 1, but for the "RANDOM" simulation.
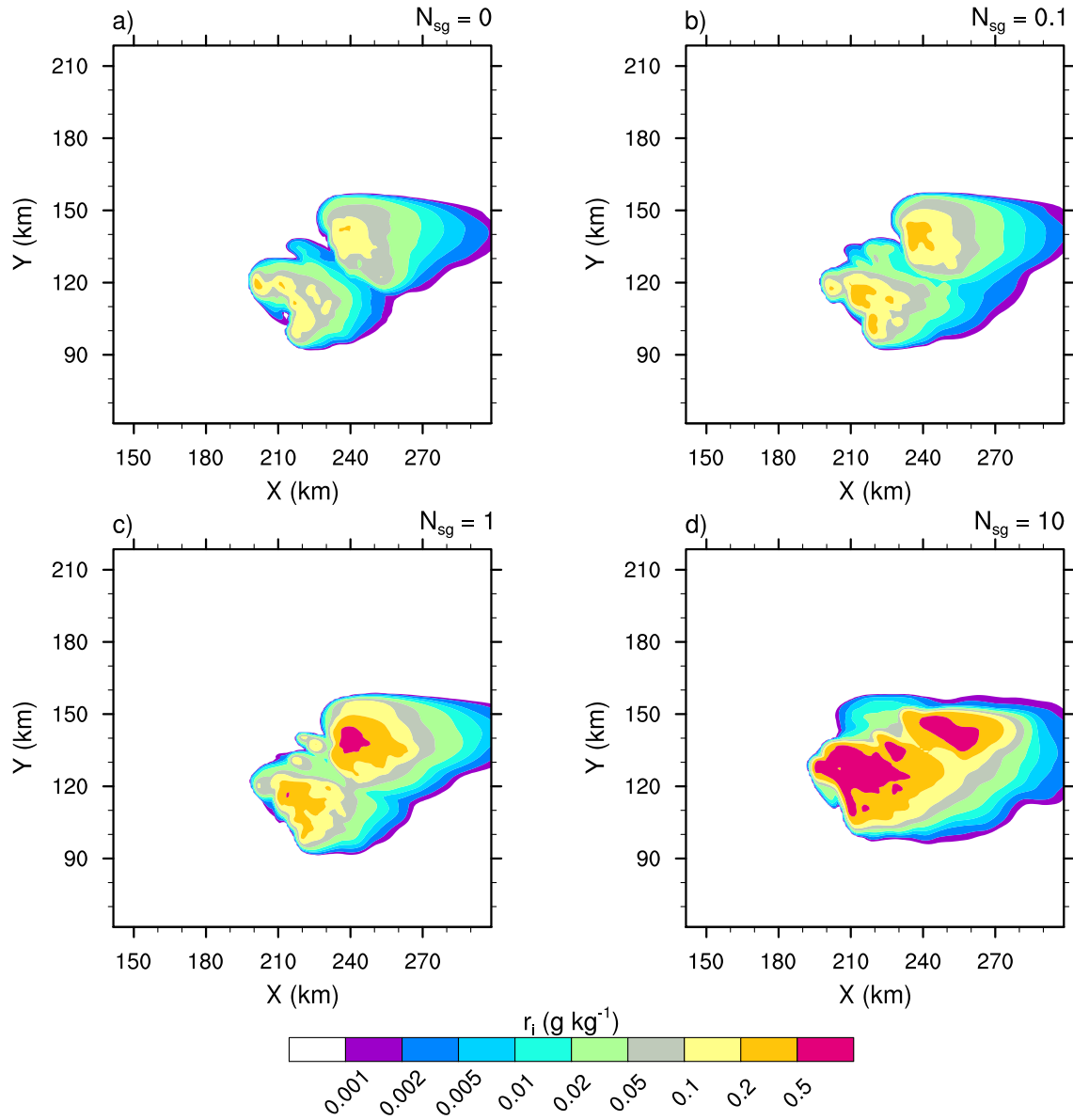
Figure 3. Mixing ratios of the cloud ice (r_i in log scale) of the STERAO simulations at 12 km height, where a) to d) refer to cases with $\mathcal{N}_{sg}$=0.0, 0.1, 1.0 and 10.0 ice fragments per collision, respectively. The plots are for a fraction of the computational domain.
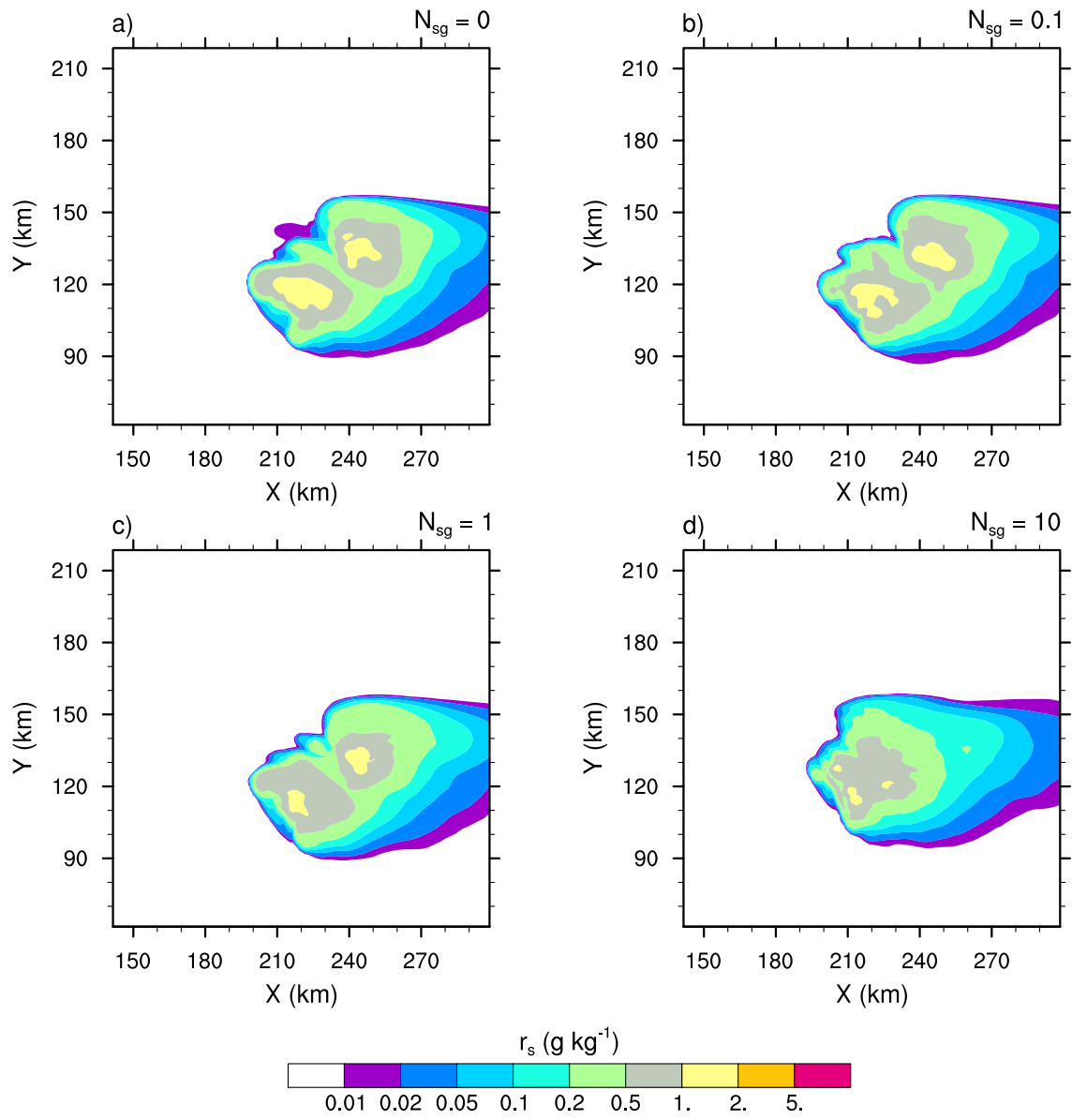
Figure 4. Same as Fig. 3 but for the mixing ratios of snow-aggregates (r_s).
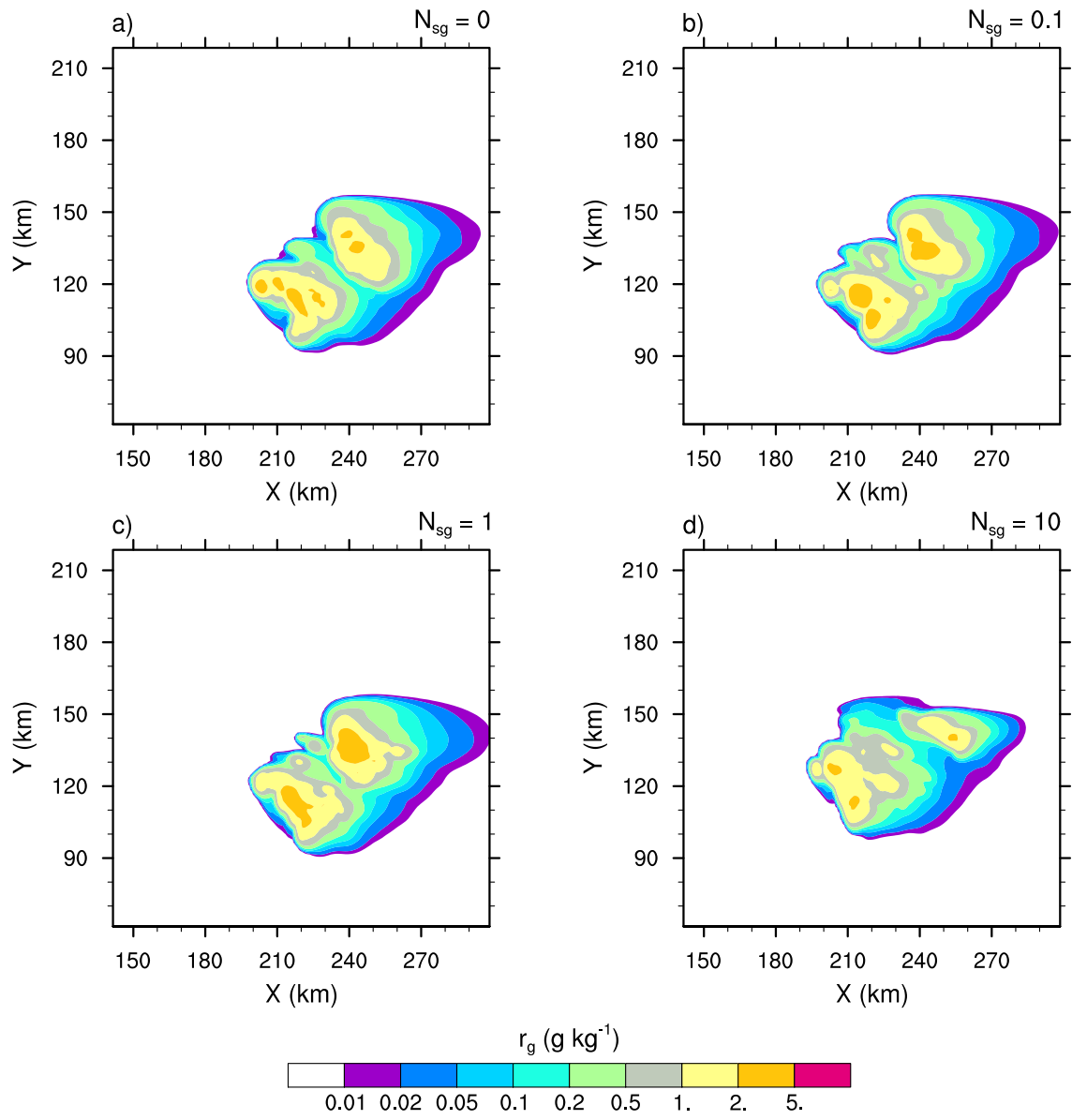
Figure 5. Same as Fig. 3 but for the mixing ratios of graupel (r_g).
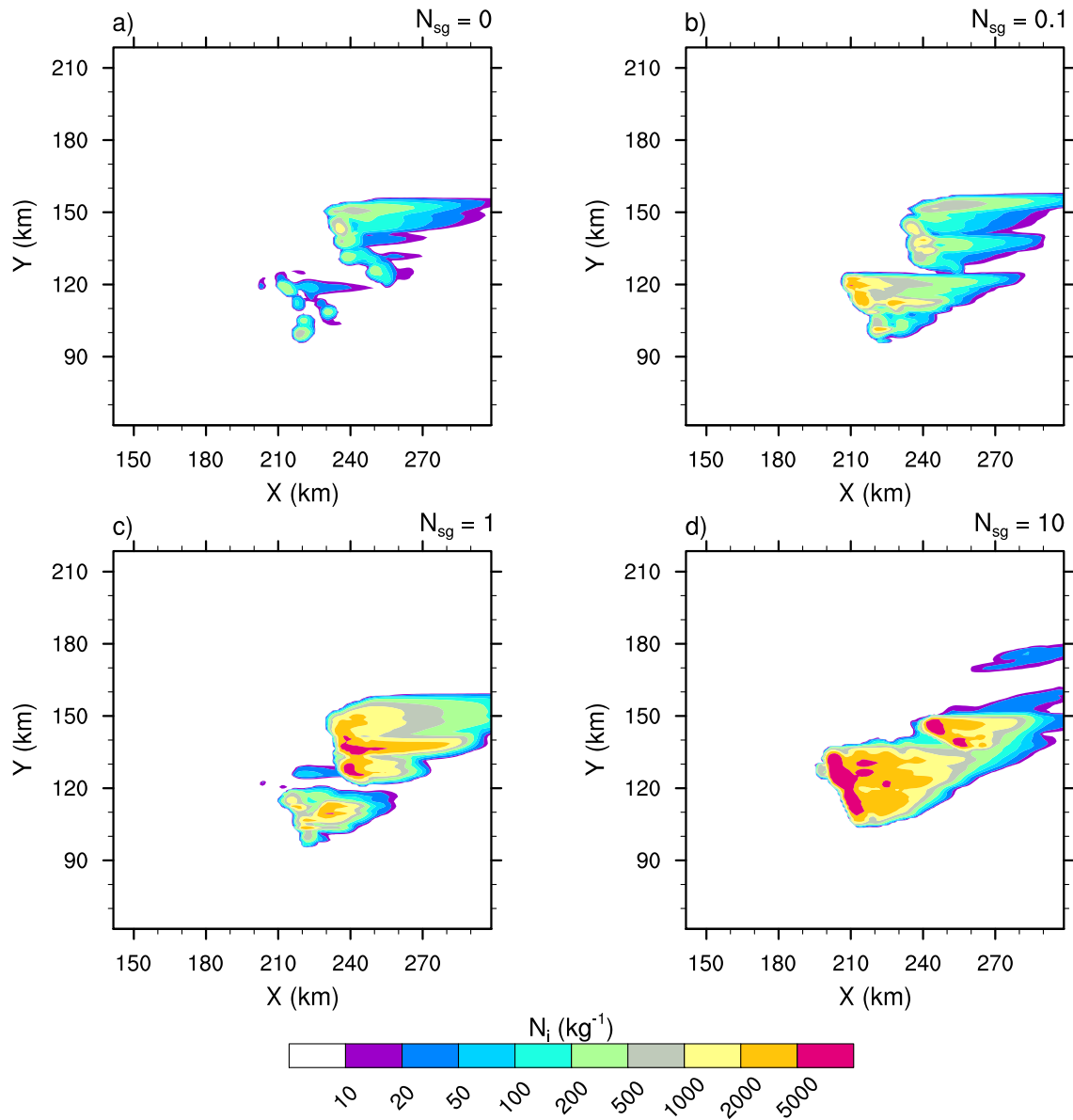
Figure 6. Number concentration of the cloud ice (N_i in log scale) of the STERAO simulations at 15 km height, where a) to d) refer to cases with $\mathcal{N}_{sg}$=0.0, 0.1, 1.0 and 10.0 ice fragments per collision, respectively. The plots are for a fraction of the computational domain.
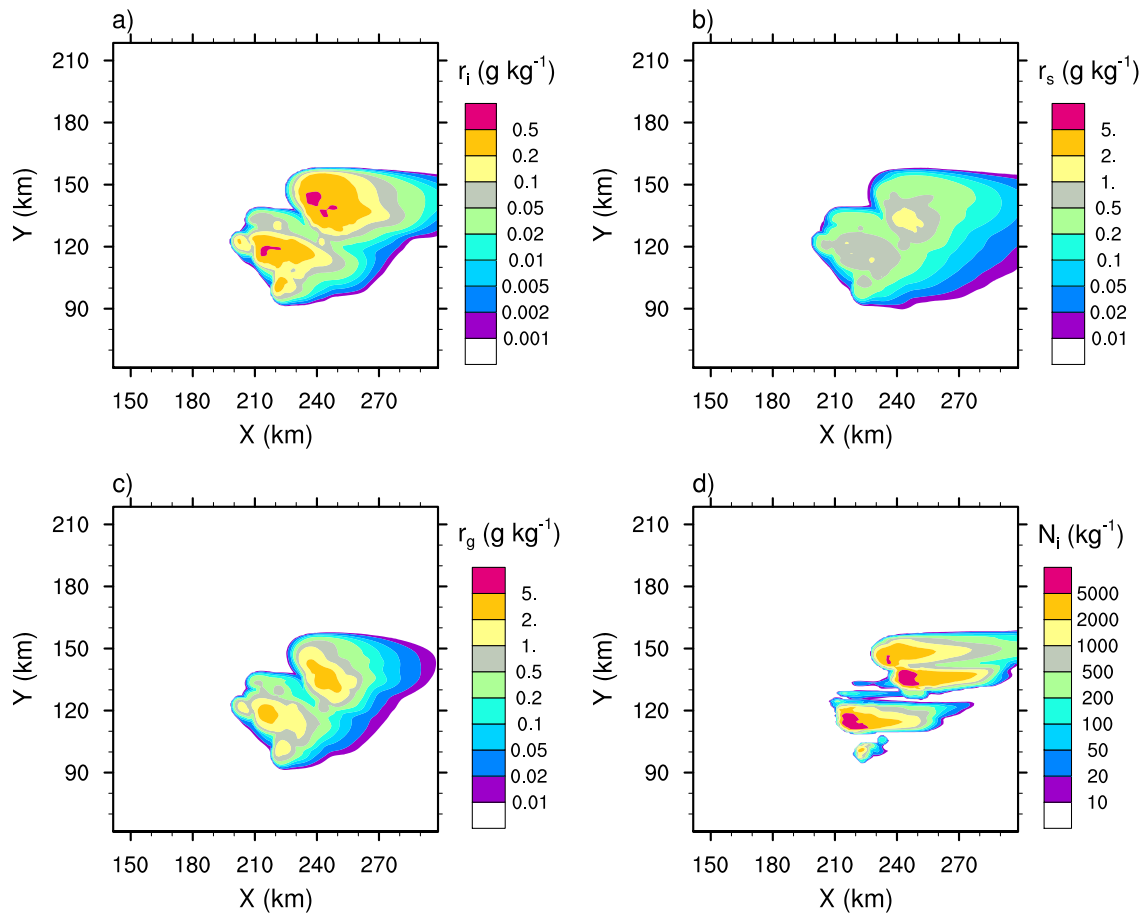
Figure 7. "RANDOM" case of the STERAO simulations showing the mixing ratios of a) the cloud ice (r_i), b) the snow-aggregates (r_s), and c) the graupel (r_g) at 12 km height. Plot d) refers to the number concentration of the cloud ice crystals (N_i) at 15 km height. The plots are for a fraction of the computational domain.
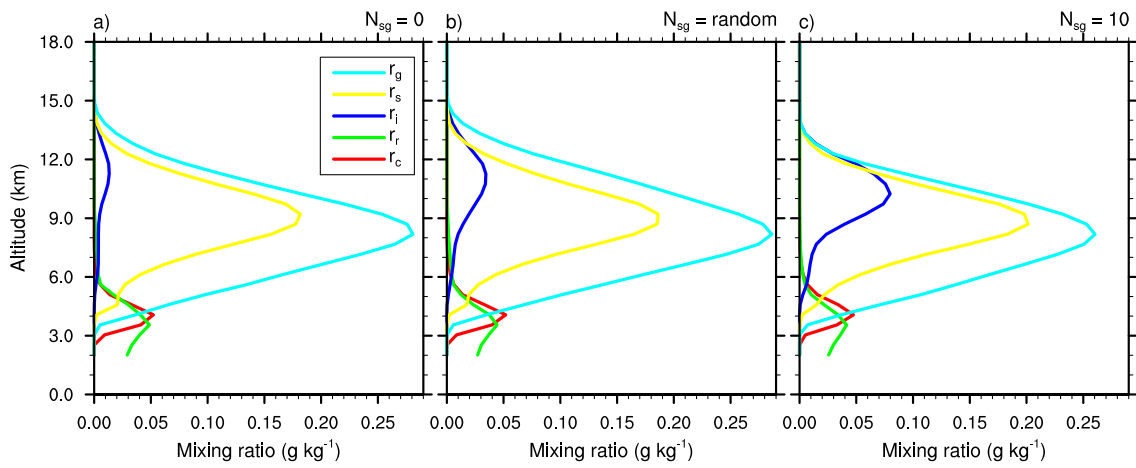
Figure 8. Mean profiles of condensate mixing ratios r_c, r_r, r_i, r_s and r_g ; in g kg^{-1}) of the STERAO simulations corresponding to a) the $\mathcal{N}_{sg}$=0.0 case, b) the "RANDOM" case and c) the case with $\mathcal{N}_{sg}$ = 10.0.
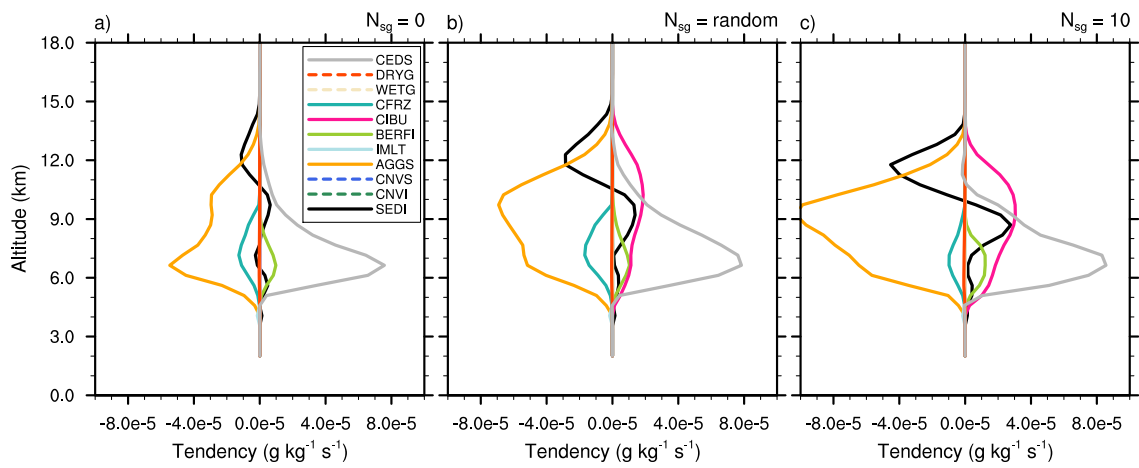
Figure 9. Mean microphysics profiles of cloud ice mixing ratio tendencies of the STERAO simulations corresponding to a) the $\mathcal{N}_{sg} = 0.0$ (no CIBU) case, b) the "RANDOM" case and c) the case with $\mathcal{N}_{sg} = 10.0$. The dashed lines are associated with processes having no significant impact on these budgets.
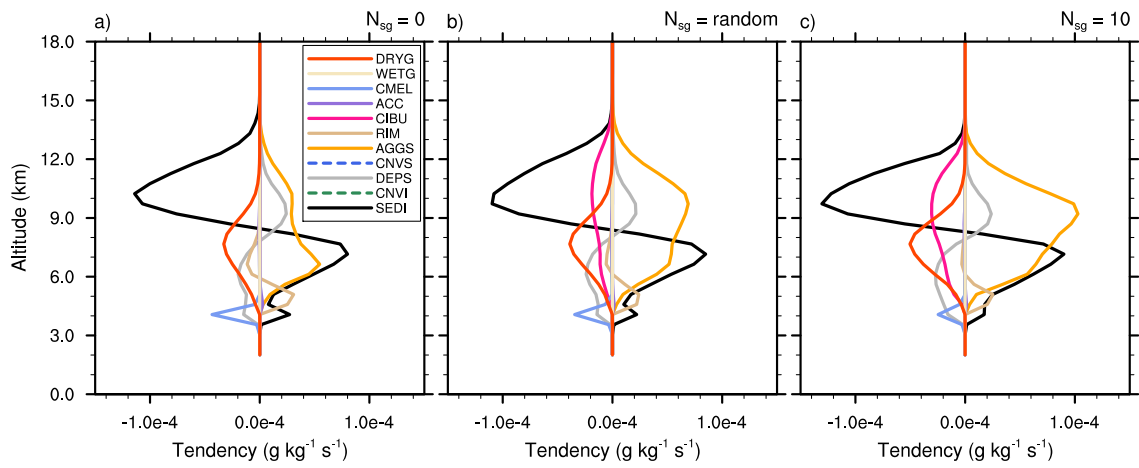
Figure 10. Same as Fig. 9 but for snow-aggregates.
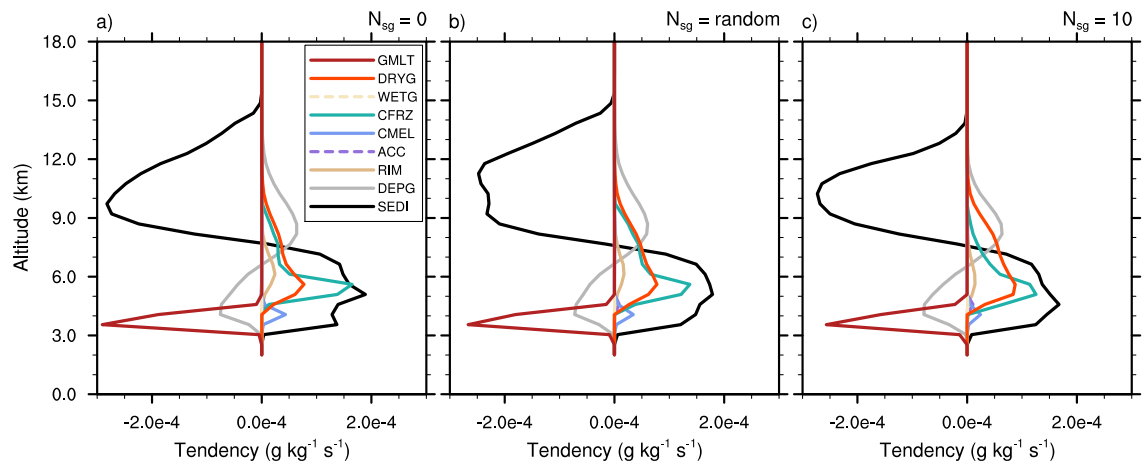
Figure 11. Same as Fig. 9 but for graupel.
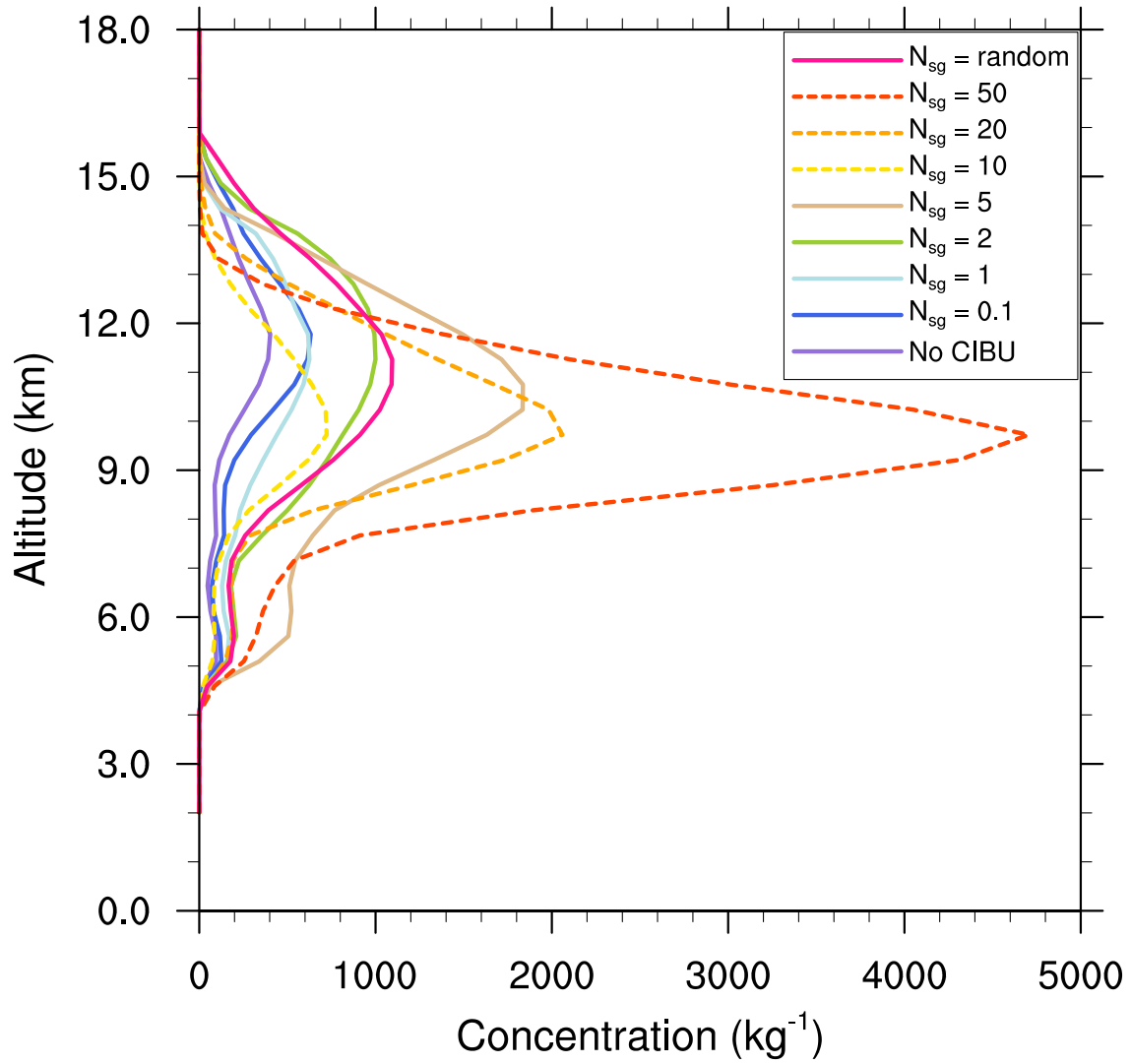
Figure 12. Mean profiles of the cloud ice crystal concentrations N_i (g kg^{-1}) of the STERAO simulations corresponding to different values of $\mathcal{N}_{sg}$ (see the legend for details). The profiles drawn with a dashed line have been divided by 10 to fit into the plot.
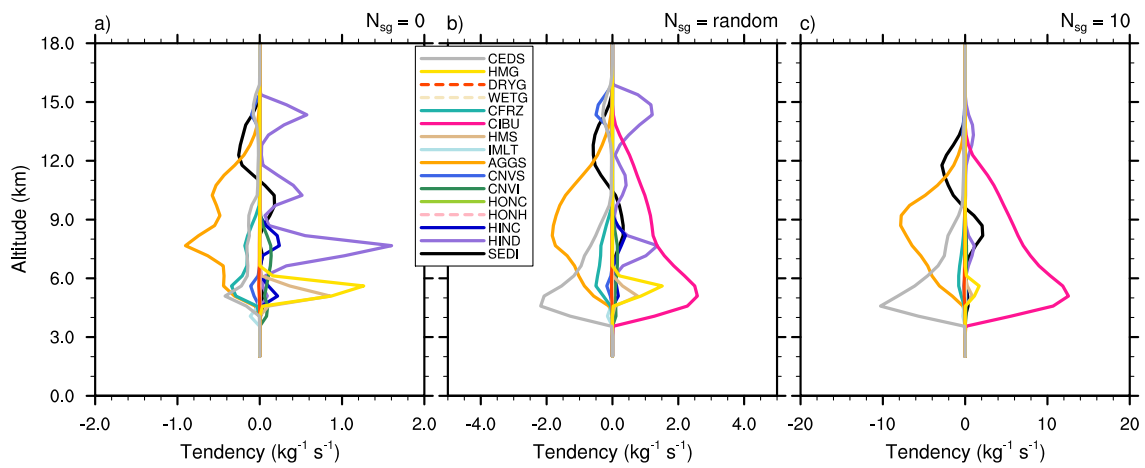
Figure 13. Mean microphysics profiles of the cloud ice crystal concentration tendencies of the STERAO simulations corresponding to a) the $\mathcal{N}_{sg} = 0.0$ (no CIBU) case, b) the "RANDOM" case and c) the case with $\mathcal{N}_{sg} =$ 10.0 (Note that the horizontal scale increases from a) to c)). The dashed lines of the list box are associated with processes having no significant impact on these budgets.
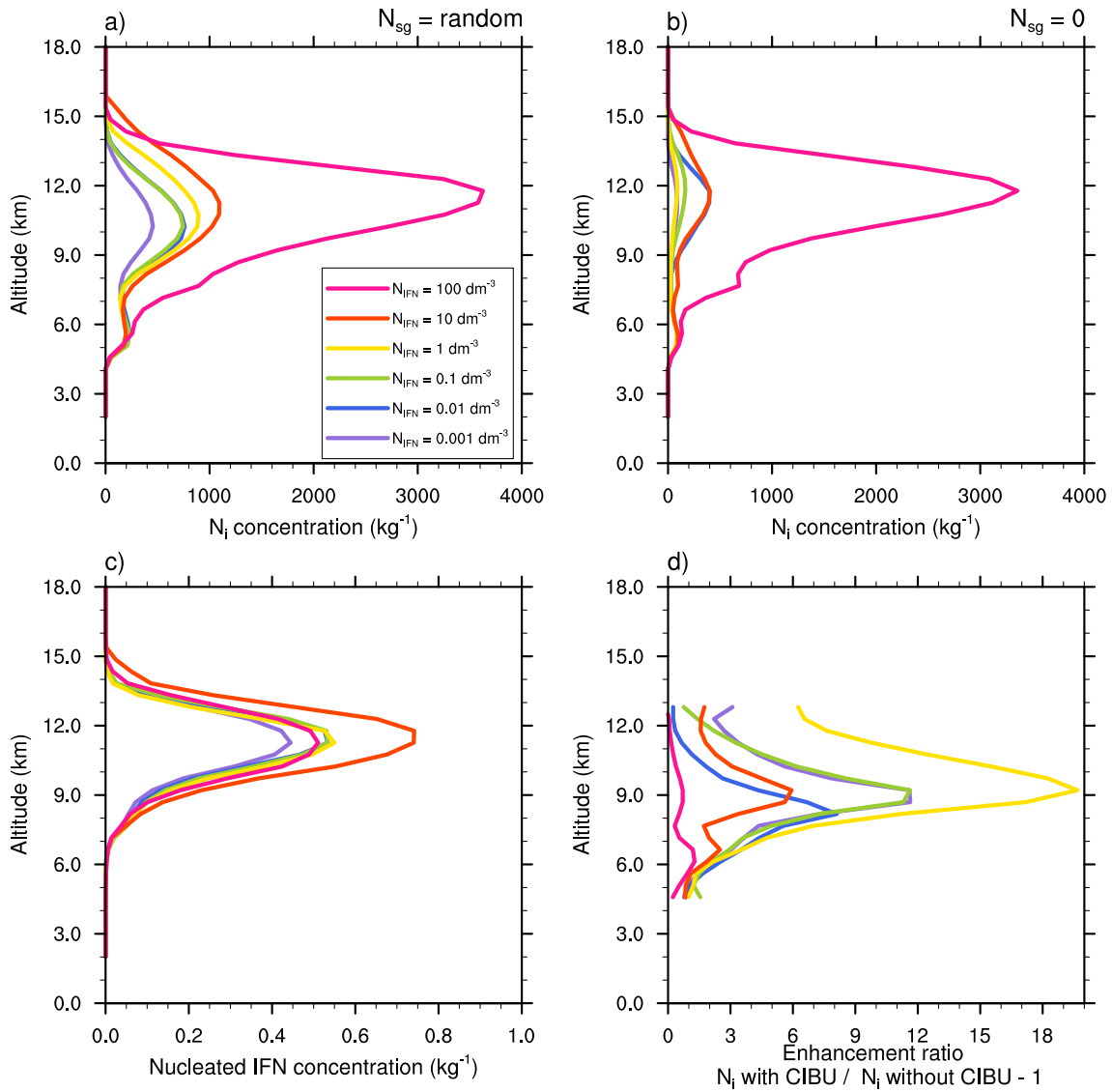
Figure 14. Mean profiles of cloud ice crystal concentration for 6 decades of initial IFN concentrations from 100 dm^{-3} to 0.001 dm^{-3} of the STERAO simulations corresponding to a) the CIBU simulation and "RANDOM" case and b) the non-CIBU simulation. The mean profiles of the nucleated IFN concentrations are plotted in c) after rescaling to fit the [0.0-1.0] range. The rough estimate of CIBU enhancement factor of Ni is plotted in d) as a function of the initial IFN concentrations.